Supplementary Information (SI) for Nanoscale.

Supplementary Information for

Selenium-Modified In_2O_3 Photoanode: Oxygen Vacancy-Mediated "Defect Capture-Interface Transport" and Extended Light Absorption for Efficient Photoelectrochemical Water Splitting

Changxue Dong[a], Jinwei Chen[a,b,*], Qiuyan Chen[a], Han Tan[a], Kun Jiang[c,*], Ruilin Wang[a,b,*]

[a] College of Materials Science and Engineering, Sichuan University, Chengdu 610065, China.

[b] Engineering Research Center of Alternative Energy Materials & Devices, Ministry of Education, Chengdu, 610065, China.

[c] Department of Integrated Traditional Chinese and Western Medicine, West China Hospital, Sichuan University, Chengdu 610041, PR China

*Corresponding Authors.

E-mail: jwchen@scu.edu.cn (Jinwei Chen), dr_jiangkun@126.com (Kun Jiang), rl.wang@scu.edu.cn (Ruilin Wang)

Experimental Section

Chemicals and materials.

Indium sulfate ($In_2(SO_4)_3$, ≥99.99%), selenium (Se, 99.9%), aniline ($C_6H_5NH_2$, ≥99.99%), sodium sulfate anhydrous (Na_2SO_4, 99.99%), and sodium sulfite (Na_2SO_3, 98%) were all purchased from Aladdin Industrial Corporation and used without further purification. Ultrapure Millipore water (18.25 MΩ) was used in all experiments.

Photoelectrochemical Measurements.

PEC experiments were performed on a CHI660E electrochemical work station. A three-electrode system was constructed, where the as-prepared photoanodes were used as a working electrode, the Pt piece was used as a counter electrode, and a saturated Ag/AgCl as a reference electrode.

A PLS-SXE300CBF Xe arc lamp equipped with 420 nm cut-off filter was employed as the simulated solar source. The intensity at the PEC working electrode position was adjusted to be 100 mW/cm^2 under AM 1.5G illumination. An aqueous solution of 0.5 M Na_2SO_4 was used as an electrolyte during the test. The photocurrent versus voltage (*J*-*V*) curves was determined by linear sweep voltammetry (LSV) from –0.8 to 0.8 V (vs Ag/AgCl) with a scan rate of 10 mV s^{-1}. All electrode potentials in this paper were converted to reversible hydrogen electrodes (RHE) using the Nernst equation at room temperature:

$$E_{RHE} = E_{Ag/AgCl} + 0.197 + 0.059 \times \text{pH}\ (25\ °\text{C}) \qquad \text{(equation S1)}$$

ABPE was calculated according to equation S2:

$$\text{ABPE}(\%) = \frac{[J(mA\ cm^{-2}) \times (1.23 - V_{bias})(V)}{P_{total}(mW\ cm^{-2})} \times 100\%$$

(equation S2)

IPCE was calculated according to equation S3:

$$\text{IPCE}(\%) = \frac{N_e}{N_p} \times 100\% = \frac{[J_{ph}(mA\ cm^{-2}) \times 1240}{\lambda(nm) \times P_{total}(mW\ cm^{-2})} \times 100\%$$

(equation S3)

$\eta_{surface}$ and η_{bulk} was calculated according to equation S4 and equation S5 respectively:

$$\eta_{surface.} = \frac{J_{H_2O}}{J_{Na_2SO_3}} \times 100\% \qquad \text{(equation S4)}$$

$$\eta_{\mathrm{bulk}} = \frac{J_{H_2O}}{J_{abs}} \times 100\% \quad \text{(equation S5)}$$

J_{abs} is the photocurrent density calculated by assuming 100% conversion of the absorbed photos to current density. The J_{abs} can be estimated from AM 1.5G solar spectrum and light harvesting efficiency (LHE) according to the following equations S6-7, where φAM 1.5G(λ)LHE(λ) represent the spectral distribution of power absorbed by the photoanode across the solar spectrum, visually represent the contribution of narrowing bandgap to the photocurrent density of the photoanode.:

$$J_{abs} = \int_{300}^{\lambda_e} \frac{\lambda}{1240} \varphi AM\ 1.5G(\lambda) LHE(\lambda) d\lambda \quad \text{(equation S6)}$$

$$LHE = 1 - 10^{-A(\lambda)} \quad \text{(equation S7)}$$

Instrumentations.

TEM, HRTEM, and EDX mapping were carried out on a JED-2300T Analysis Station. XRD patterns were recorded by a DX-2700 X-ray diffraction (XRD) diffractometer. XPS measurement was performed on a Thermo Scientific NEXSA of ESCALAB 250Xi with an exciting source of Al Kα = 1486.6 eV. The binding energies obtained in the XPS spectral analysis were corrected for specimen charging by referencing C 1s to 284.6 eV. photoluminescence spectra were measured on an Edinburgh FluoroLog-3 spectrofluorometer with an excitation wavelength (λ_{ex}) of 350 nm. Time-Resolved photoluminescence (TRPL)measurements were carried out on an Edinburgh FluoroLog-3 fluorescence spectrometer equipped with a xenon lamp, a monochromator for steady-state PL excitation, and a time-correlated single-photon counting unit coupled with a pulsed laser diode for time-resolved PL. UV-vis diffuse reflectance data was recorded in the spectral region of 300-900 nm with a Shimadzu UV-3600i plus absorption spectrophotometer. The work functions and valance band of photocatalysts were performed by ultraviolet photoelectron spectroscopy (UPS, Thermo Fisher NEXSA, USA).

Table S1. Structural parameters, such as interplanar distance (d), lattice parameter (a), crystallite size (D), lattice strain (ε), and dislocation density (δ), were obtained from the XRD analysis of In2O3-x and In2O3-x@In2Se3 photoanode.

Photoanode	(hkl)	d (Å)	a (Å)	D (nm)	ε ($\times10^{-3}$)	δ ($\times 10^{14}$ m^{-2})
In_2O_{3-x}	(211)	4.121	10.10	22.5	8.61	19.7
	(440)	1.788	10.12	33.3	2.53	9.01
In_2O_{3-x}@In_2Se_3	(211)	4.146	10.16	46.2	4.21	4.68
	(440)	1.790	10.13	31.9	2.64	9.84

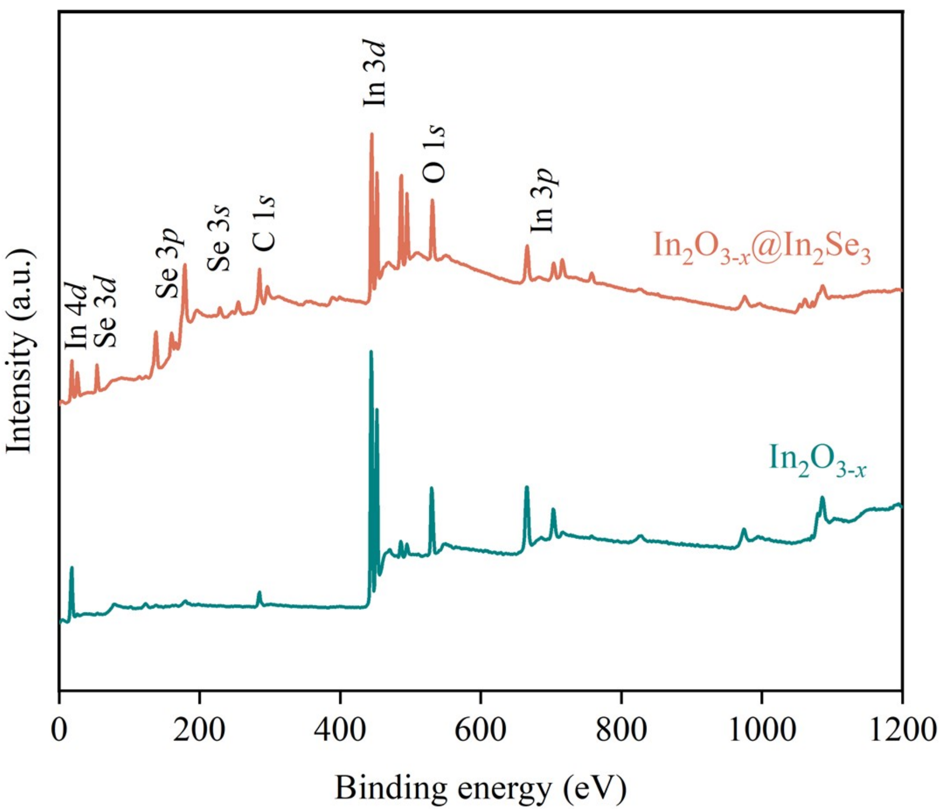

Figure S1 XPS spectra of In_2O_{3-x} and In_2O_{3-x}@In_2Se_3 photoanodes.

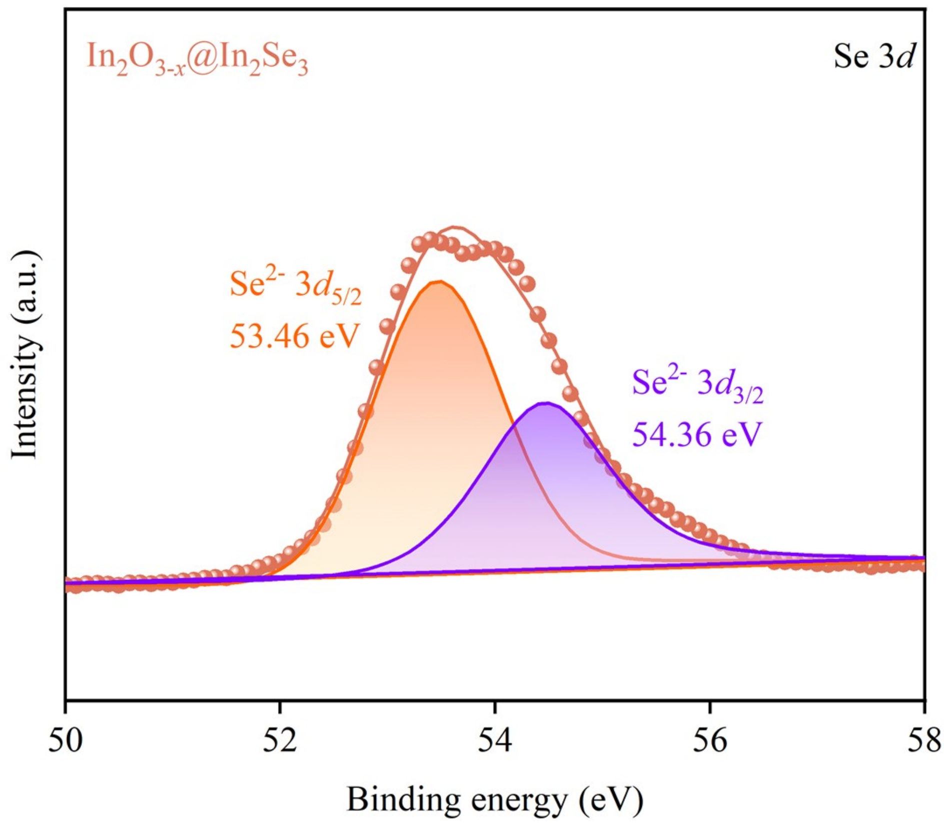

Figure S2 Se 3*d* XPS spectrum of In_2O_{3-x}@In_2Se_3 photoanode.

Table S2 The ratio of O_V/O in O 1*s* XPS spectra.

Photoanode	The ratio of O_V/O
In_2O_{3-x}	27.59 %
In_2O_{3-x}@In_2Se_3	37.96 %

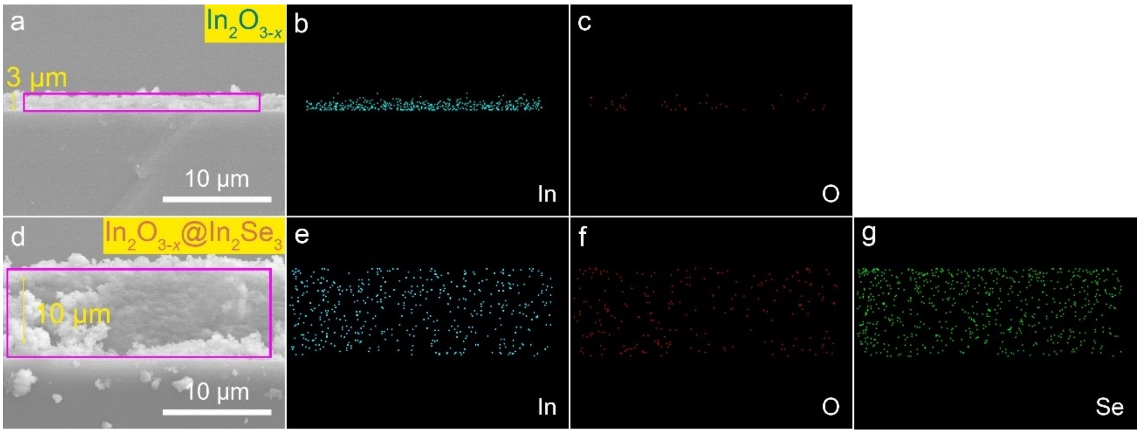

Figure S3 Cross section SEM images of (a-c) In_2O_{3-x}, (d-g) In_2O_{3-x}@In_2Se_3 photoanodes.

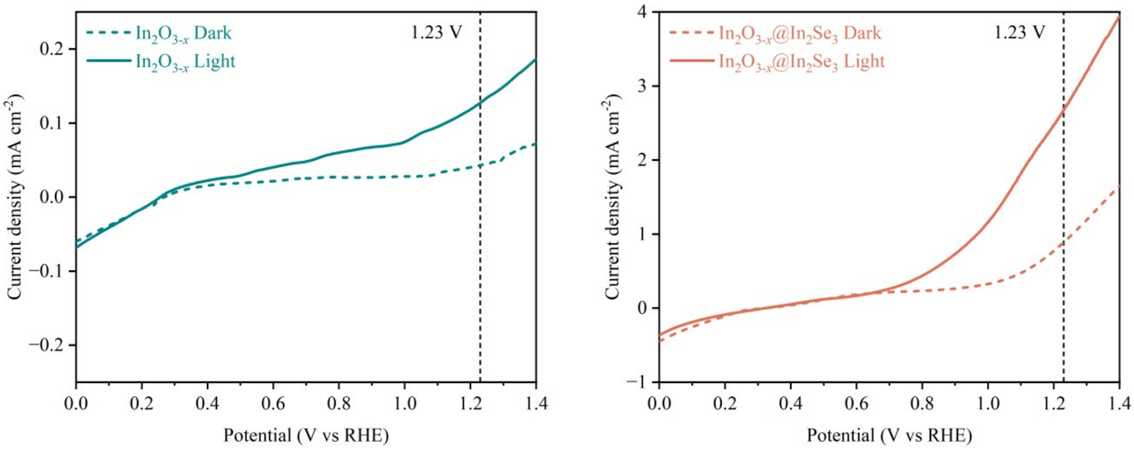

Figure S4 J-V curves for In_2O_{3-x} and In_2O_{3-x}@In_2Se_3 photoanodes under dark and light condition.

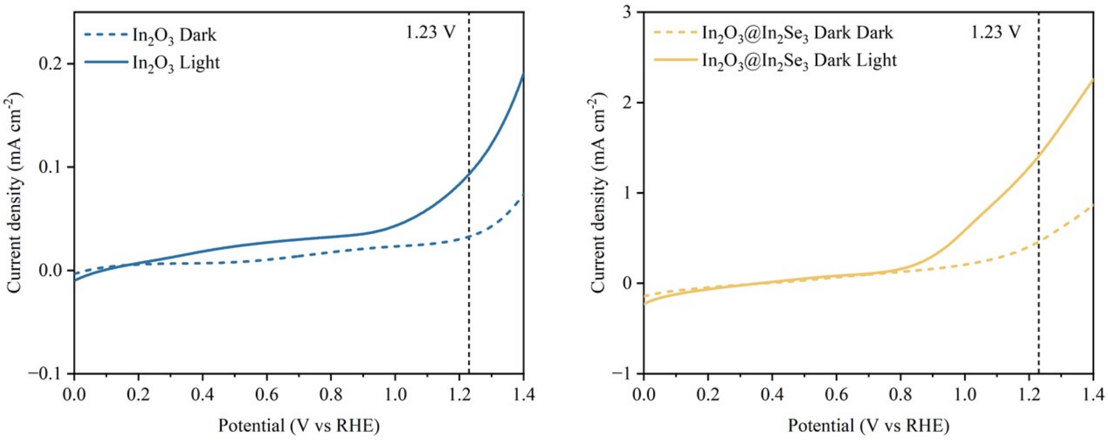

Figure S5 J-V curves for In_2O_3 and In_2O_3@In_2Se_3 photoanodes under dark and light condition.

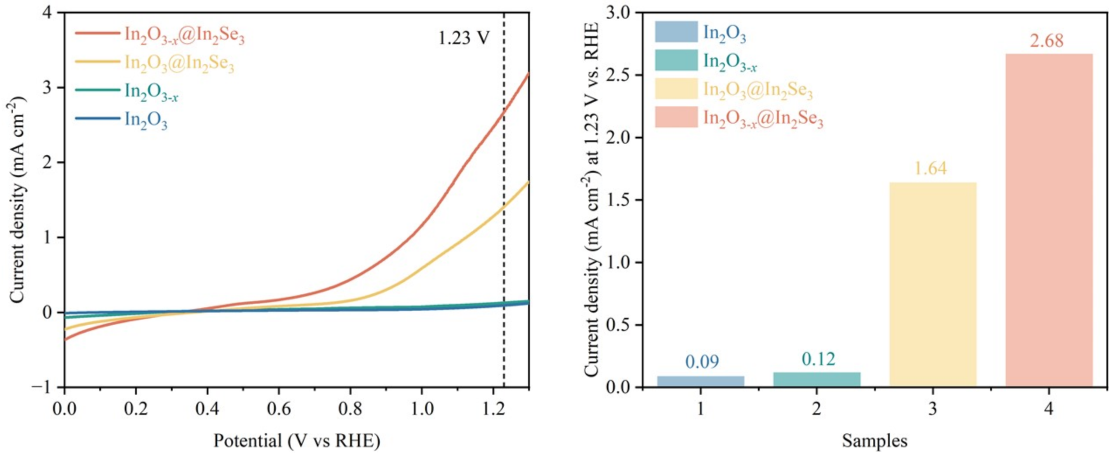

Figure S6 J-V curves and corresponding current density (mA cm^{-2}) at 1.23 V vs. RHE for as-prepared photoanodes under AM 1.5 G solar illumination.

Table S3 Recently reports of In_2O_3-based photoanodes.

Photoanode	Electrolyte	Photocurrent density (mA cm^{-2})	Monochromatic quantum yield	Ref.
α-Fe_2O_3-In_2O_3	KOH	4.5 (1.23 V vs. RHE)	22%, 360 nm	1
$BiVO_4$/In_2O_3/FeNi	Na_2SO_4	4 (1.23 V vs. RHE)	/	2
In_2O_{3-x}@In_2Se_3	Na_2SO_4	2.68 (1.23 V vs. RHE)	26.30 %, 420 nm	This work
In_2O_3/α-Fe_2O_3	KOH	2.2 (1.23 V vs. RHE)	/	3
Ti-$ZnFe_2O_4$/In_2O_3	KOH	2.2 (1.23 V vs. RHE)	29.55%, 390 nm	4
Ti-Fe_2O_3/In_2O_3	KOH	2 (1.23 V vs. RHE)	82%, 390 nm	5
20% In_2Se_3/In_2O_3(-3V)	NaOH	1.91 (1.6 V vs. RHE)	/	6
In_2O_3/CuO	NaOH	1.51 (1.6 V vs. RHE)	/	7
20% In_2Se_3/In_2O_3(+3V)	NaOH	1.29 (1.6 V vs. RHE)	/	6
20% In_2Se_3/In_2O_3(0V)	NaOH	0.99 (1.6 V vs. RHE)	/	6
In_2S_3/In_2O_3	Na_2SO_4	0.83 (1.18 V vs. RHE)	/	8
In_2O_3@In_2S_3	NaOH	0.53 (1.23 V vs. RHE)	/	9

$In_2O_3@In_2S_3$	Na_2SO_4	0.14 (1.23 V vs. RHE)	/	10

Table S4 Recently reports of other oxide-based heterojunction photoanodes.

Photoanode	Electrolyte	Photocurrent density (mA cm^{-2})	Monochromatic quantum yield	Ref.
In_2O_{3-x}@In_2Se_3	Na_2SO_4	2.68 (1.23 V vs. RHE)	26.30 %, 420 nm	This work
NiS/WO_3/SnS_2	Na_2SO_4	2.78 (1.23 V vs. RHE)	45%, 300 nm	11
$CoSe_2$/WO_3@Si-4	Na_2SO_4	2.62 (1.23 V vs. RHE)	/	12
WO_3/In_2S_3/CQDs	Na_2SO_4	2.13 (1.23 V vs. RHE)	17%, 400 nm	13
$BiVO_4$/Bi_2S_3@bio-Cr_2O_3	KPi	6.00 (1.23 V vs. RHE)	79.3%, 360 nm	14
M-CoS/$BiVO_4$	K-Borate	5.22 (1.23 V vs. RHE)	70%, 420 nm	15
CoS/Mo-$BiVO_4$	PBS	4.5 (1.23 V vs. RHE)	47.48%, 350 nm	16
FeOOH@1T-MoS_2@$BiVO_4$	PBS	4.02 (1.23 V vs. RHE)	78%, 420 nm	17
NiFe-LDH/CdS/$BiVO_4$	KOH	3.1 (1.23 V vs. RHE)	78.6%, 450 nm	18
$BiVO_4$/Bi_2S_3	Na_2SO_4	2.71 (1.23 V vs. RHE)	/	19
E-$BiVO_4$/MoS_2	Na_2SO_4 and PBS	2.11 (1.23 V vs. RHE)	40.9%, 340 nm	20
ZIS@TiO_2 NT-EA	NH_4F in EG	3.89 (1.23 V vs. RHE)	40.9%, 300 nm	21

TiO_2@$Cd_{0.5}Zn_{0.5}S/Co_2P$	NaOH	3.62 (1.23 V vs. RHE)	41.6%, 360 nm	22
TiO_2/In_2S_3/NiFeP	KOH	3.18 (1.23 V vs. RHE)	/	23
TiO_2-PSS-CdS	Na_2S and Na_2SO_3	3.07 (1.23 V vs. RHE)	/	24
Cu_2SnS_3-S/TiO_2	Na_2SO_4	2.54 (1.23 V vs. RHE)	/	25
TiO_2/CdS/g-C_3N_4	Na_2SO_3 and Na_2S	2.38 (1.23 V vs. RHE)	/	26
CdS/C/TiO_2	Na_2SO_4	1.55 (1.23 V vs. RHE)	63.59%, 400 nm	27

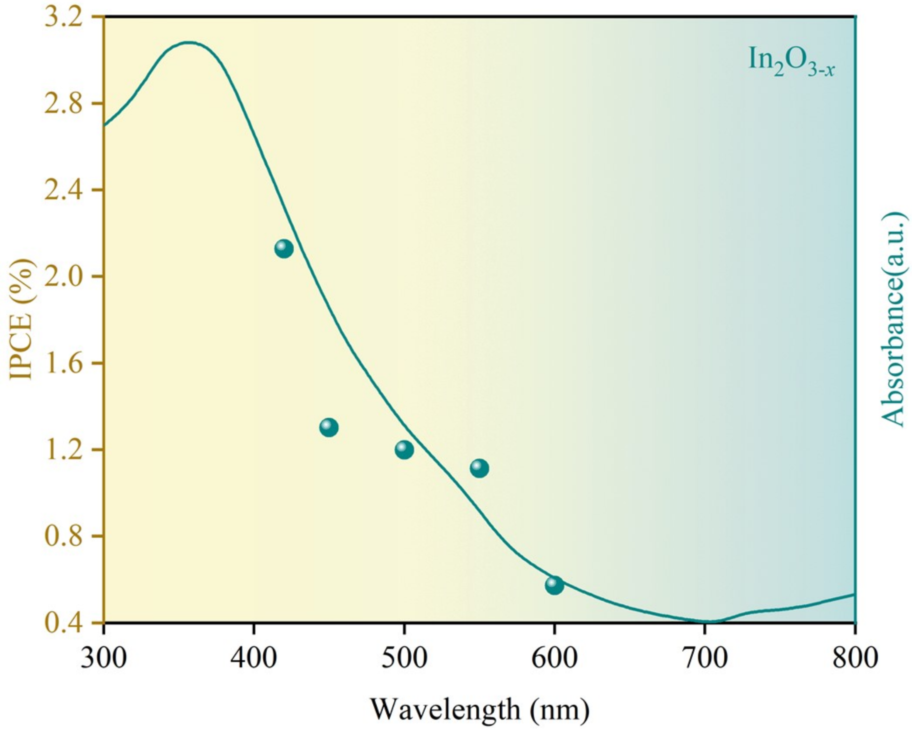

Figure S7 The UV-Vis absorption and corresponding incident photon-to-current conversion efficiency (IPCE) curves of In2O3-x photoanode.

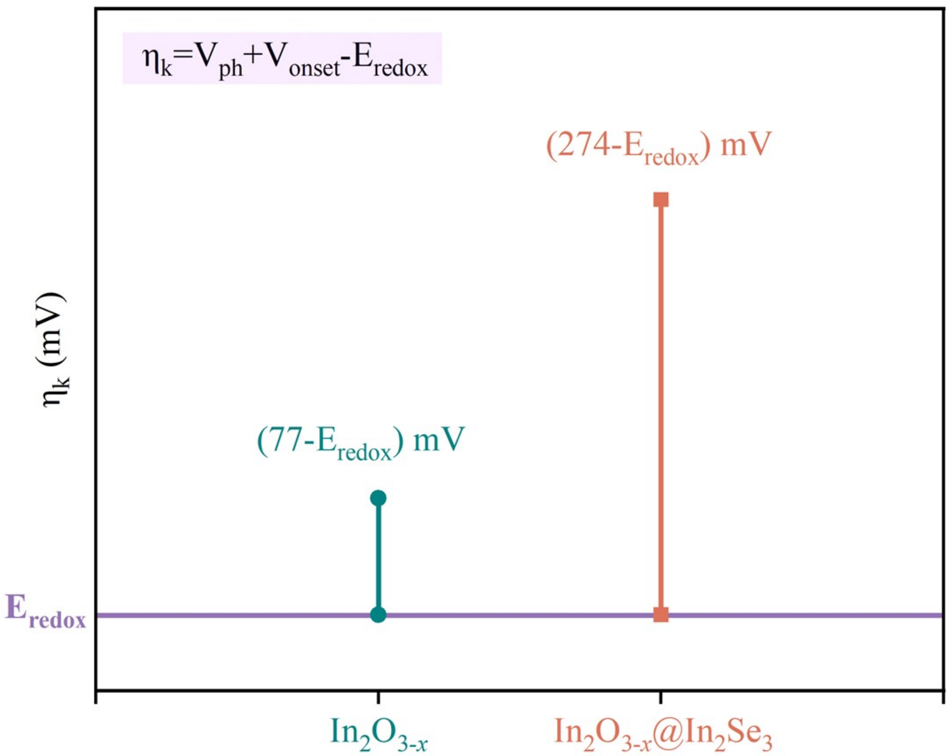

Figure S8 Kinetic overpotential (η_k) of as-prepared photoanodes.

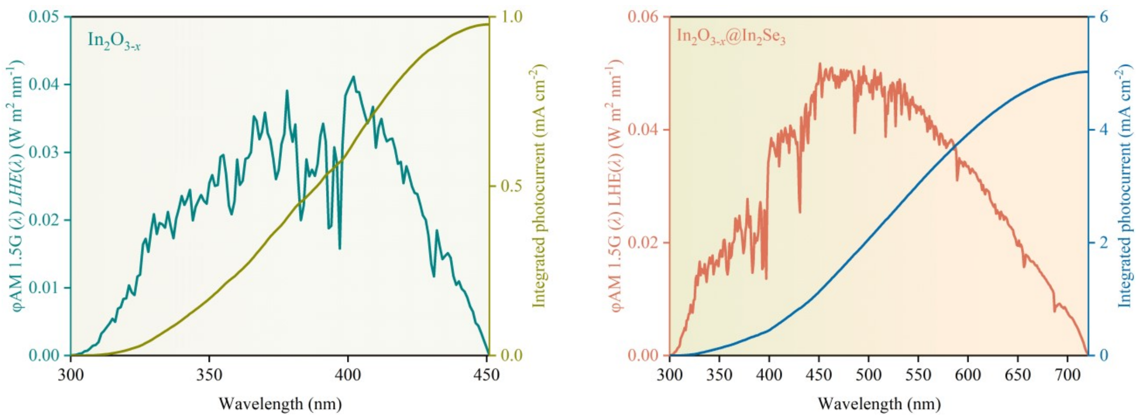

Figure S9. The calculated current density fluxes and the integrated current densities (J_{abs}).

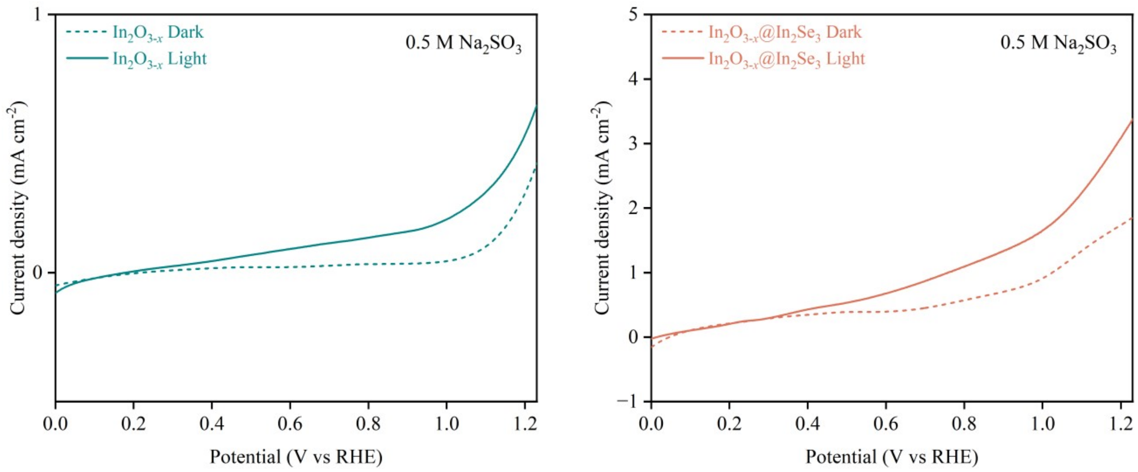

Figure S10 J-V curves for In_2O_{3-x} and In_2O_{3-x}@In_2Se_3 photoanodes in 0.5 M Na_2SO_3 electrolyte under dark and light condition.

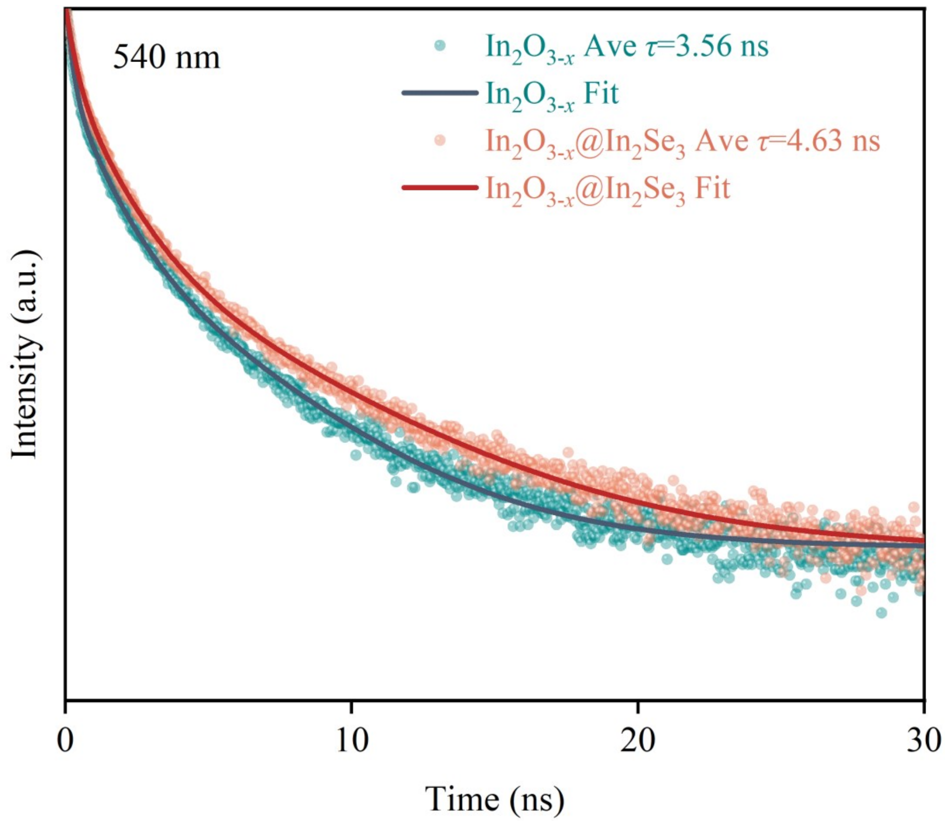

Figure S11 Transient photoluminescence decay curves of photoanodes at PL emission peak of 540 nm

Table S5 Transient photoluminescence decay data of In_2O_{3-x} and In_2O_{3-x}@In_2Se_3 photoanodes (PL emission peak of 460 nm).

Photoanode	τ_1 (ns)	A_1	τ_2 (ns)	A_2	τ_3 (ns)	A_3	τ_{ave} (μs)
In_2O_{3-x}	0.31	0.20	1.46	0.47	7.60	0.33	6.17
In_2O_{3-x}@In_2Se_3	3.96	0.34	0.69	0.06	22.37	0.60	20.65

Table S6 Transient photoluminescence decay data of In_2O_{3-x} and In_2O_{3-x}@In_2Se_3 photoanodes (PL emission peak of 540 nm).

Photoanode	τ_1 (ns)	A_1	τ_2 (ns)	A_2	τ_3 (ns)	A_3	τ_{ave} (μs)
In_2O_{3-x}	0.20	0.12	1.12	0.39	4.13	0.49	3.56
In_2O_{3-x}@In_2Se_3	0.31	0.12	1.34	0.43	5.47	0.45	4.63

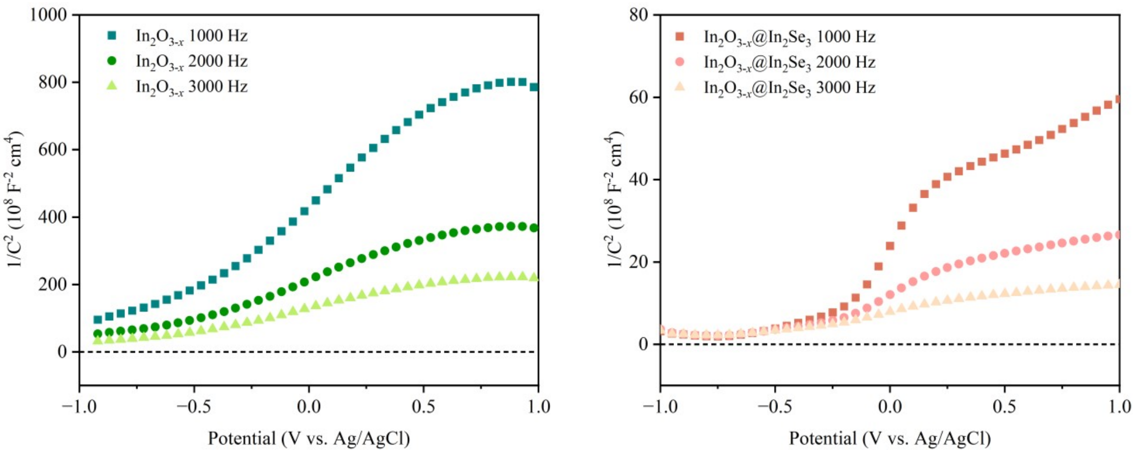

Figure S12 Mott-Schottky plots of photoanodes under different frequency.

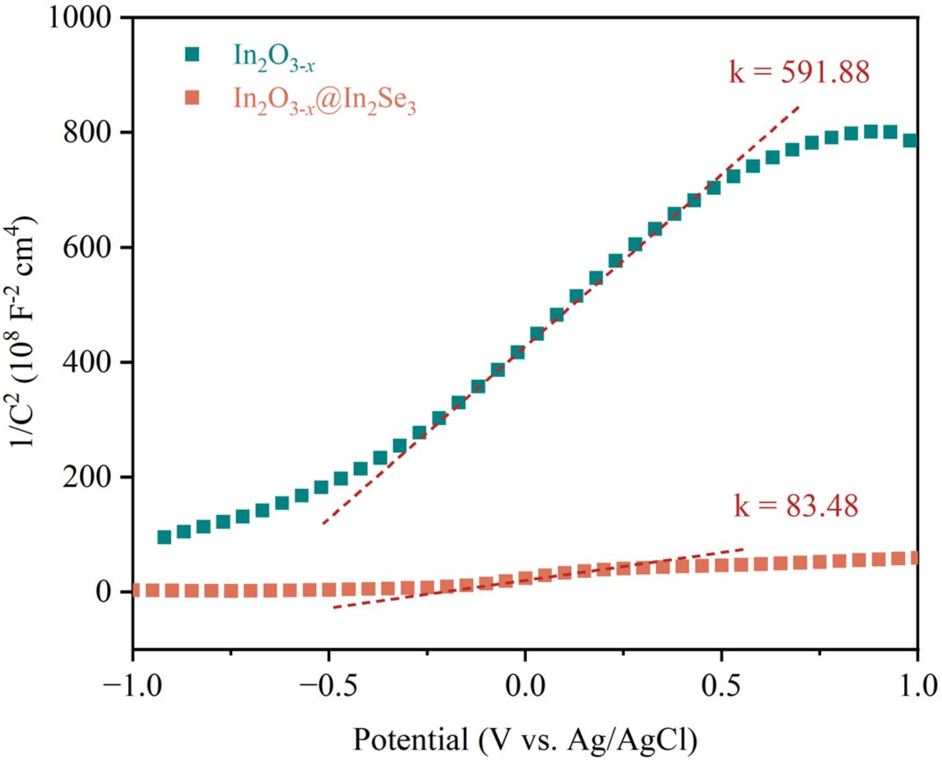

Figure S13 Mott-Schottky plots of photoanodes under 1000 Hz.

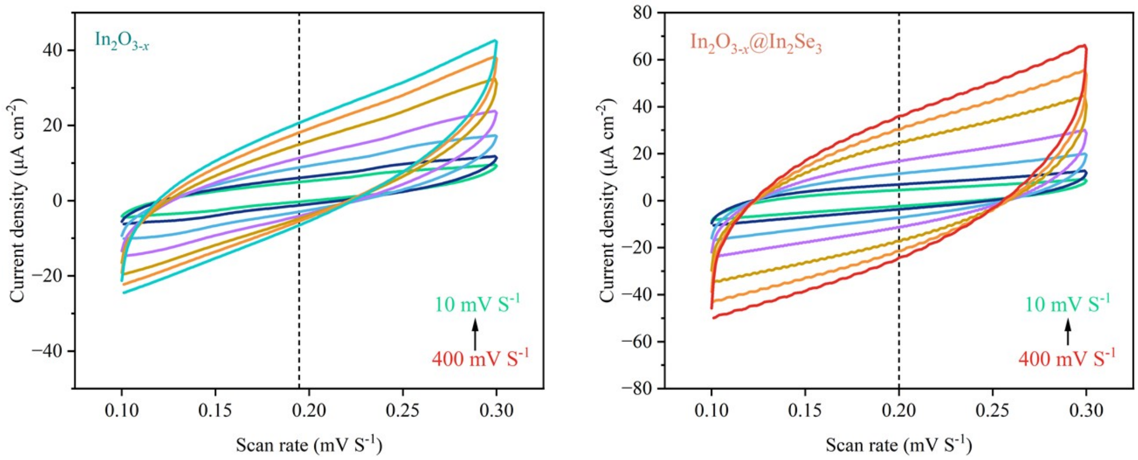

Figure S14 Cyclic voltammograms (CV) spectra of photoanodes. The CV measurement was performed in the non-Faradaic region with a potential range of 0.7-0.9 V vs. RHE at scan rates of 10, 20, 50, 100, 200, 300 and 400 mV s^{-1}.

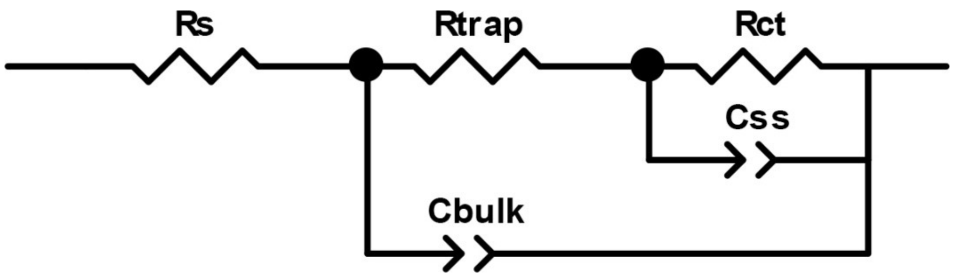

Figure S15 Equivalent circuit model. R_s refers to the whole series resistance ascribed to the electrolyte, external contact and conductive substrate, R_{trap} refers to the charge trapping resistance in the semiconductor; R_{ct} refers to the charge transfer resistance of semiconductor/electrolyte interface; C_{bulk} refers to the capacitance in the depletion layer; C_{ss} refers to the capacitance of semiconductor/electrolyte interface.

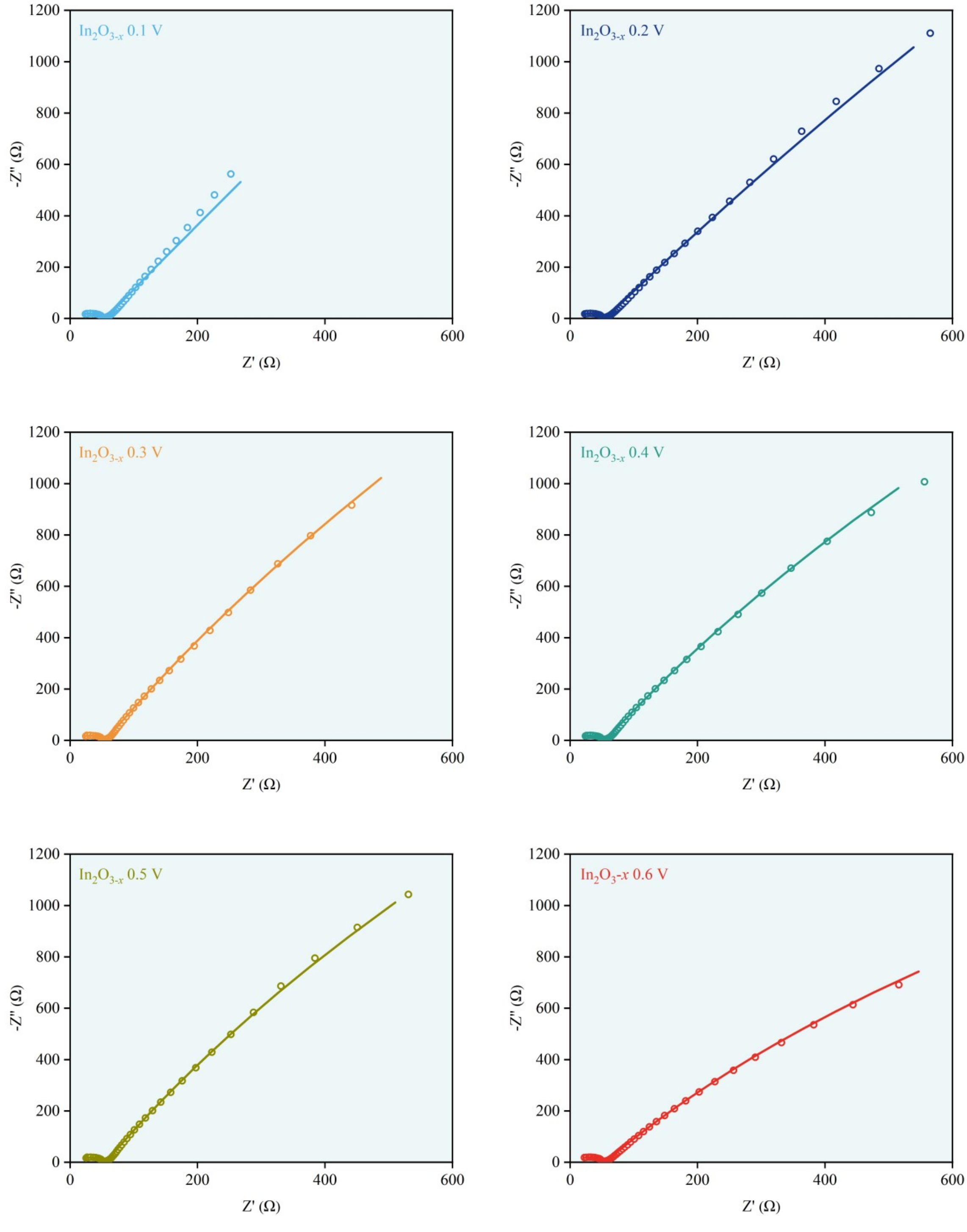

Figure S16 Nyquist plot and fitting curves of In_2O_{3-x} photoanode.

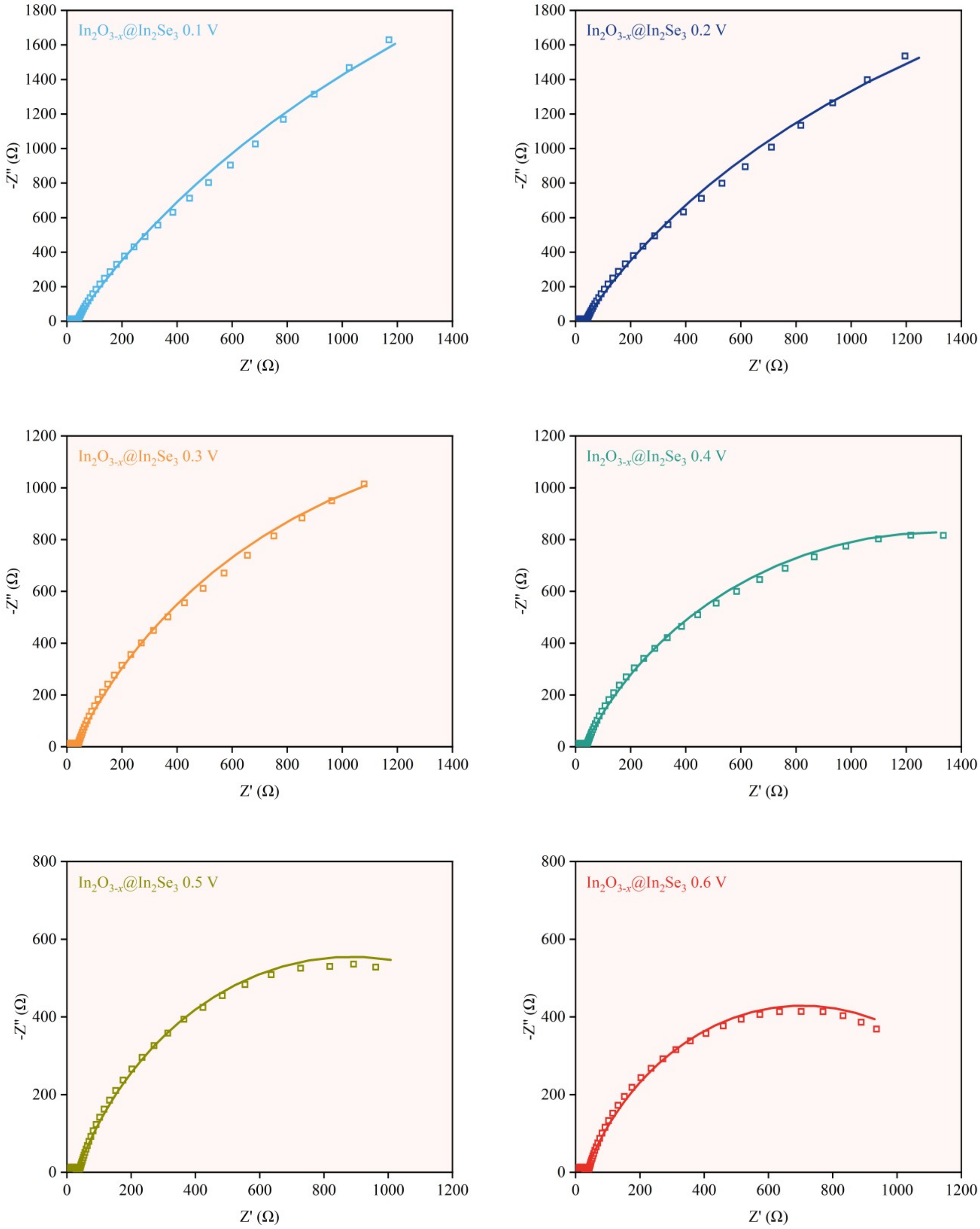

Figure S17 Nyquist plot and fitting curves of In_2O_{3-x}@In_2Se_3 photoanode.

Table S7 Parameters of the fitted nyquist plots of photoelectrochemical impedance spectroscopy (PEIS).

Sample	Applied potential (V vs. RHE)	R_s (Ω)	R_{trap} (Ω)	R_{ct} (Ω)	C_{bulk} (nF)	C_{ss}(μF)
In_2O_{3-x}	0.7	5.145	50.49	85362	89.599	206.53
	0.8	5.688	50.00	29632	81.191	213.46
	0.9	4.897	50.62	14864	97.445	205.18
	1.0	4.637	50.83	12265	100.500	214.38
	1.1	5.741	50.17	11333	94.099	203.29
	1.2	4.922	50.04	5563	68.005	239.61
In_2O_{3-x}@In_2Se_3	0.7	4.670	26.35	8278	11.671	113.51
	0.8	5.214	25.74	6515	13.534	109.29
	0.9	5.141	25.68	3507	16.232	134.30
	1.0	4.349	26.88	2579	14.935	103.22
	1.1	4.507	26.48	1709	14.805	124.08
	1.2	4.211	27.00	1348	11.529	119.88

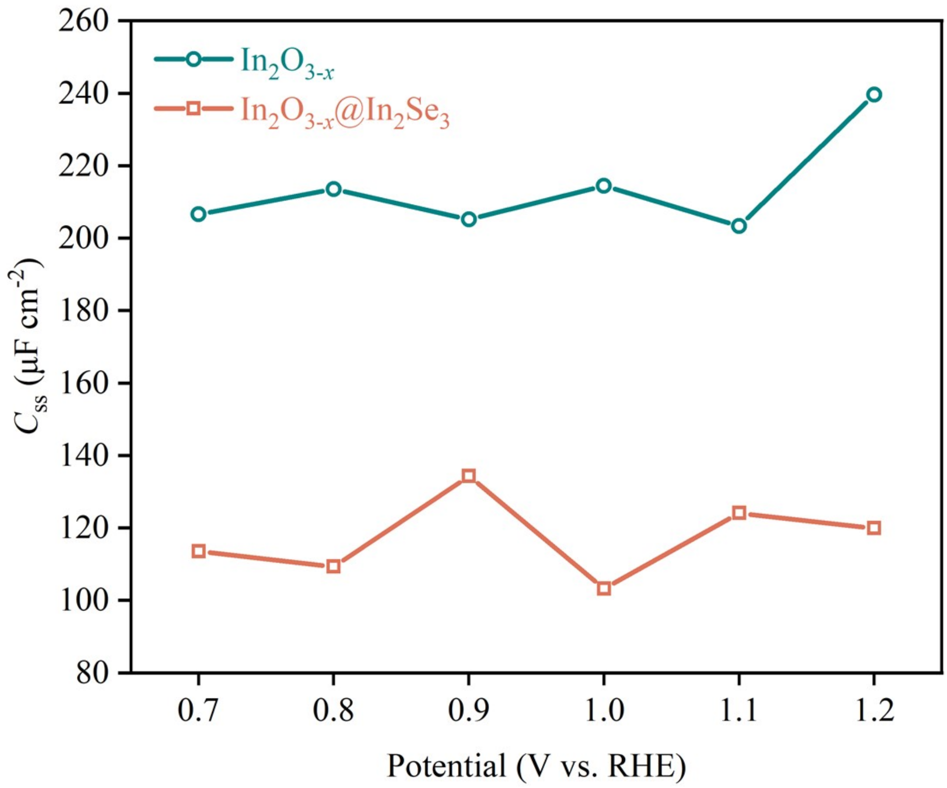

Figure S18 Charge transfer resistance of In_2O_{3-x} and In_2O_{3-x}@In_2Se_3 photoanodes.

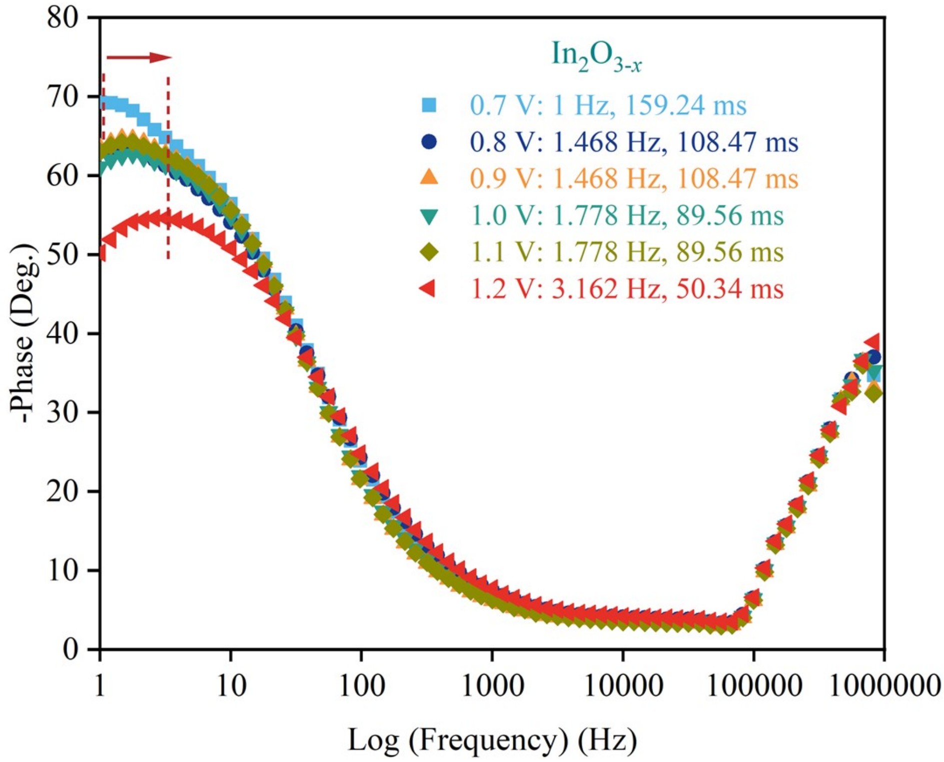

Figure S19 Bode spectra of $In_2O_{3\text{-}x}$ photoanode.

Table S8 The transit times (τ_n) calculated using f_{max} from the bode plots.

Sample	Applied potential (V vs. RHE)	f_{max} (Hz)	τ_n(ms)
In_2O_{3-x}	0.7	1	159.24
	0.8	1.468	108.47
	0.9	1.468	108.47
	1.0	1.778	89.56
	1.1	1.778	89.56
	1.2	3.162	50.34
In_2O_{3-x}@In_2Se_3	0.7	14.68	10.85
	0.8	14.68	10.85
	0.9	17.78	8.96
	1.0	26.1	6.10
	1.1	26.1	6.10
	1.2	31.62	5.04

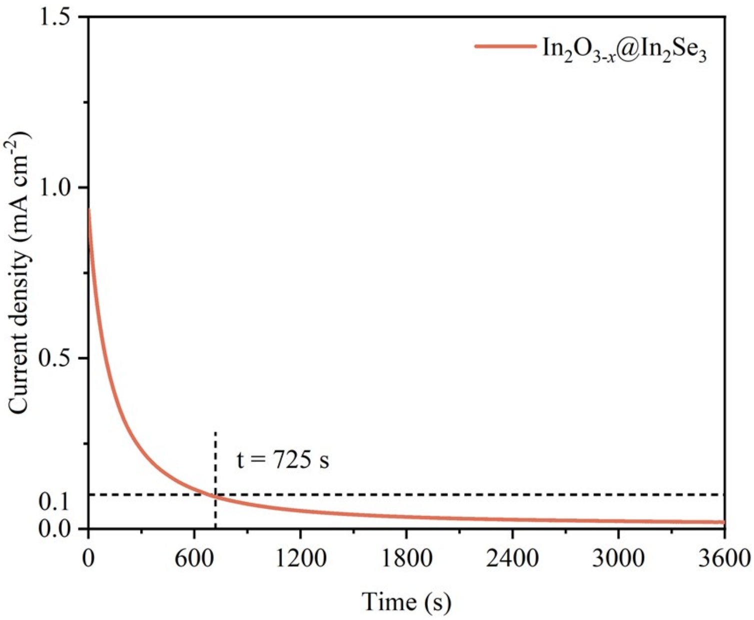

Figure S20 J-T curves for $In_2O_{3\text{-}x}$@In_2Se_3 and used $In_2O_{3\text{-}x}$@In_2Se_3 photoanodes at 1.0 V vs. RHE in 0.1 M Na_2SO_4 electrolyte under AM 1.5 G solar illumination.

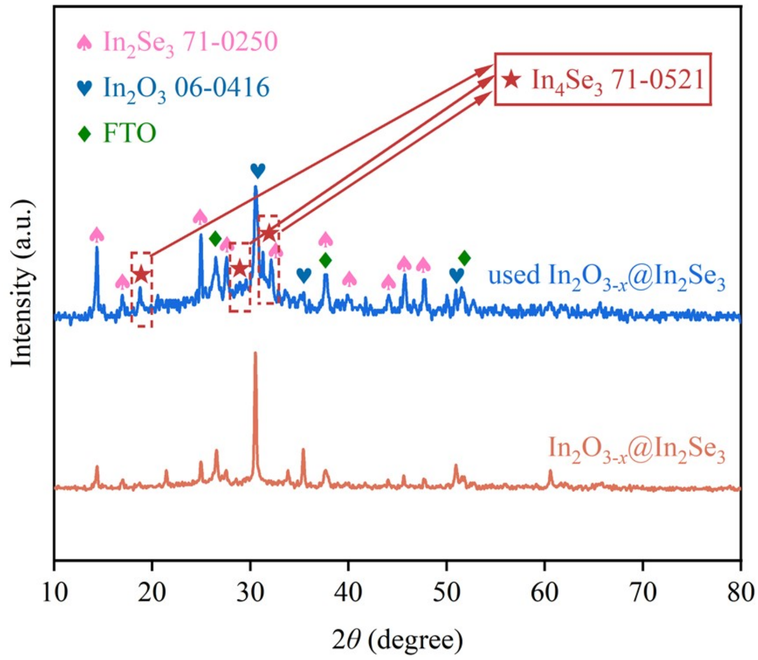

Figure S21 XRD pattern of In_2O_{3-x}@In_2Se_3 and used In_2O_{3-x}@In_2Se_3 photoanodes.

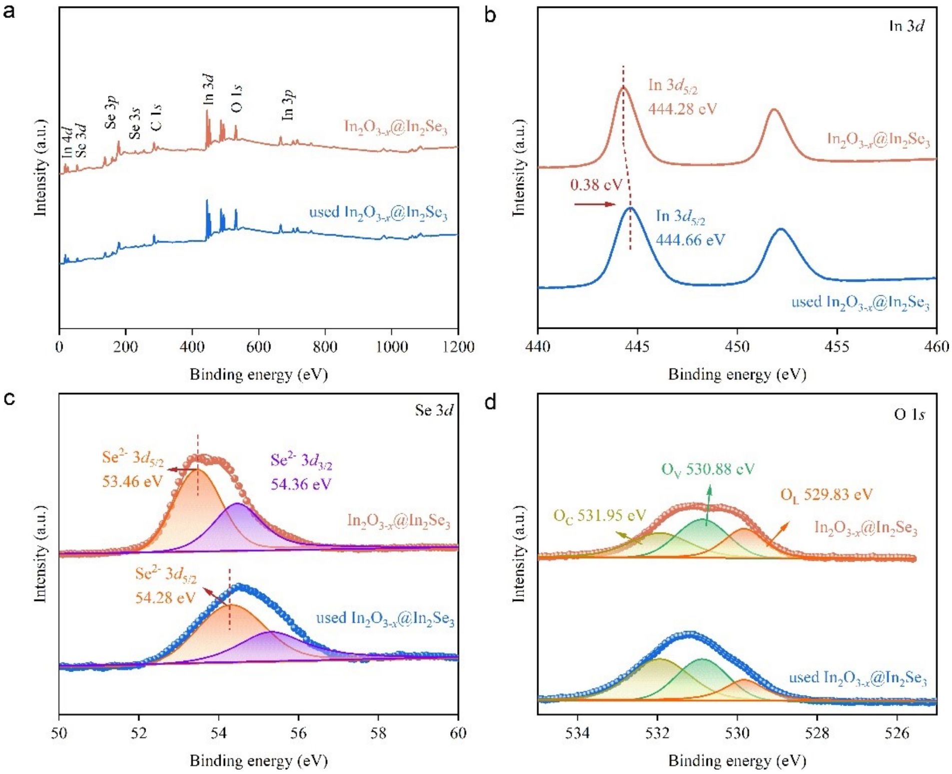

Figure S22 (a) Total XPS spectra, (b) In 3*d*, (c) Se 3*d*, and (d) O 1*s* XPS spectra of In_2O_{3-x}@In_2Se_3 and used In_2O_{3-x}@In_2Se_3 photoanodes.

Table S9 The ratio of O_V/O in O 1*s* XPS spectra.

Photoanode	The ratio of O_V/O
In_2O_{3-x}@In_2Se_3	37.96 %
used In_2O_{3-x}@In_2Se_3	34.26 %

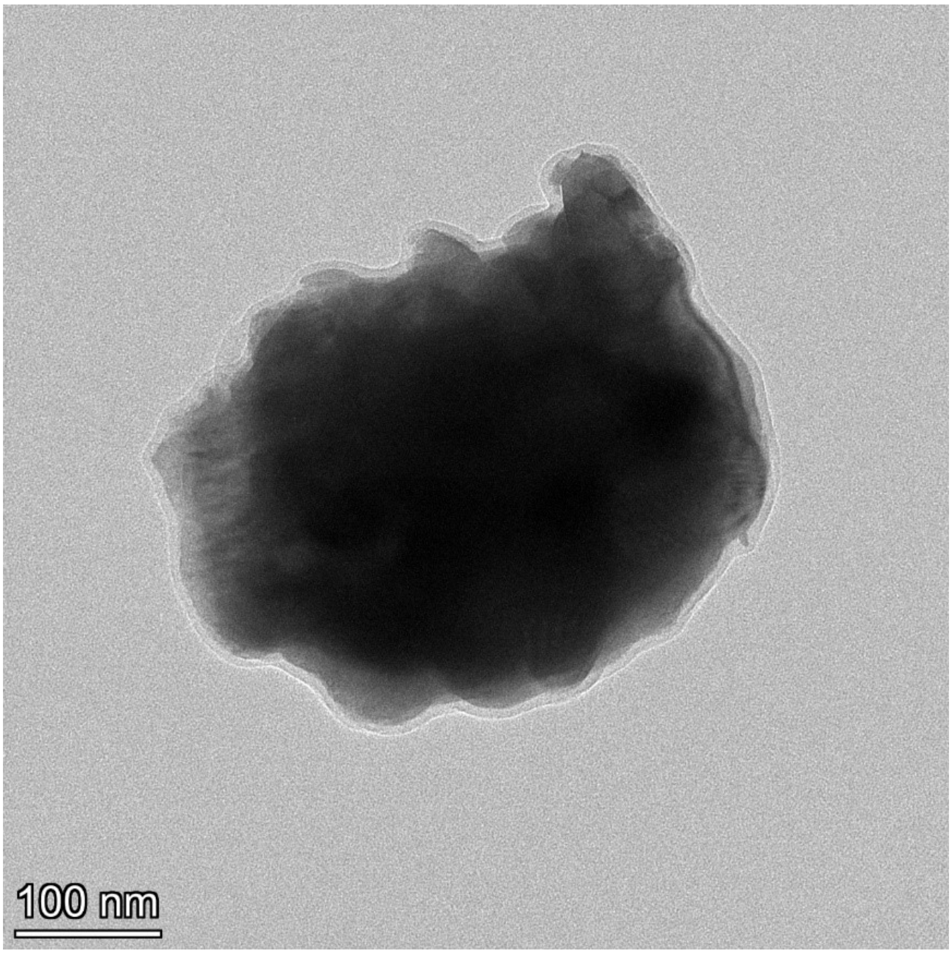

Figure S23 TEM image of In_2O_{3-x}@In_2Se_3-PANI photoanode.

References

1. M.-H. Ji, Y.-X. Chen, R. Chen, K.-X. Li, H.-P. Zhao, H.-Y. Shi, H.-L. Wang, X. Jiang and C.-Z. Lu, *International Journal of Hydrogen Energy*, 2024, **51**, 66-77.
2. D. Yin, X. Ning, Q. Zhang, P. Du and X. Lu, *Journal of Colloid and Interface Science*, 2023, **646**, 238-244.
3. Y. Zhou, R. Sun, H. Li, X. Liu, C. Song and D. Wang, *International Journal of Hydrogen Energy*, 2024, **83**, 236-245.
4. K. Ba, Y. Li, Y. Liu, Y. Lin, D. Wang, T. Xie and J. Li, *Journal of Colloid and Interface Science*, 2023, **649**, 492-500.
5. Y. Li, Q. Wu, Y. Chen, R. Zhang, C. Li, K. Zhang, M. Li, Y. Lin, D. Wang, X. Zou and T. Xie, *Applied Catalysis B: Environmental*, 2021, **290**.
6. L. Shi, D. Benetti, F. Li, C. Harnagea, Q. Wei and F. Rosei, *Journal of Materials Chemistry A*, 2024, **12**, 29989-29997.
7. L. Shi, D. Benetti, Q. Wei and F. Rosei, *Small*, 2023, **19**.
8. M. D. Sharma, C. Mahala and M. Basu, *ACS Applied Nano Materials*, 2020, **3**, 11638-11649.
9. H. Xu, H. Chen, S. Chen, K. Wang and X. Wang, *International Journal of Hydrogen Energy*, 2021, **46**, 32445-32454.
10. B. R. Lee, S. Choi, W. S. Cheon, J. W. Yang, M. G. Lee, S. H. Park and H. W. Jang, *Electronic Materials Letters*, 2022, **18**, 391-399.
11. J. He, J. Wang, J. Wan, X. Wang, C. Feng, Q. Zhou, Q. Lan, H. Zhang and Y. Wang, *Journal of Colloid and Interface Science*, 2025, **693**.
12. L. Zhang, K. Liao, J. Liu, P. Yang, X. Chen, Z. Zhong, J. Li, H. Yang, Y. Li and Y.-N. Liu, *Langmuir*, 2025, **41**, 5347-5354.
13. Z. Liu, Z. Xu, S. Bai, S. Jia, D. Li, Y. Feng, R. Luo and A. Chen, *International Journal of Hydrogen Energy*, 2025, **163**.
14. Y. Su, Y. Yu, T. Xue, K. Teng, Y. Fan, J. Lin, C. Liu, Q. Qu and L. Li, *Chemical Engineering Journal*, 2025, **517**.
15. D. Li, X. Chen, M. Shao, S. Hou, J. Guo, H. Jin, H. Yang, G. Chen and Y. Huang, *Journal of Materials Chemistry A*, 2025, **13**, 22652-22659.
16. Y. Guan, X. Gu, Q. Deng, S. Wang, Z. Li, S. Yan and Z. Zou, *Inorganic Chemistry*, 2023, **62**, 16919-16931.
17. L. Yu, K. Xue, H. Luo, C. Liu, H. Liu, H. Zhu and Y. Zhang, *Chemical Engineering Journal*, 2023, **472**.
18. G. Dong, T. Chen, F. Kou, F. Xie, C. Xiao, J. Liang, C. Lou, J. Zhuang and S. Du, *Nanomaterials*, 2024, **14**.
19. D. Yu, Y. Xiong, H. Wu, P. Yang, H. Shi, L. Huang, Y. Wu, Y. Zhang and P. Xiao, *The Journal of Physical Chemistry C*, 2023, **127**, 2340-2348.
20. Z. Peng, Y. Su, I. Ennaji, A. Khojastehnezhad and M. Siaj, *Chemical Engineering Journal*, 2023, **477**.
21. H. Wang and G. L. Song, *ChemCatChem*, 2024, **16**.
22. X. Liu, Y. Xiong, X. Yao, Y. Che, D. Kurbanjan and H. Du, *Electrochimica Acta*, 2025, **529**.
23. M. Zhang, J. Xie, P. Yang, P. Peng, Y. Su, X. Pang, H. Wang, Y. Xiang, C. Huang and X. Lu, *International Journal of Hydrogen Energy*, 2025, **148**.
24. H. Zhang, B. Zhang, L. Zou, J. You and S. Lin, *Applied Surface Science*, 2025, **711**.

25. A. Chen, C. Chen, S. Shao, Y. Lian, Y. Du, Y. Gao, J. Yi and W. Zheng, *Dalton Transactions*, 2025, **54**, 10710-10718.

26. M. F. Mohamad Noh, N. A. Arzaee, J. Safaei, S. H. Norisham, W. A. S. Wan Razali, A. Nadzri, M. N. Harif, M. S. Bahrudin, A. Z. Arsad, F. I. Za'abar, C. C. Fat, Y. B. Kar, J. Huang and A. W. Mahmood Zuhdi, *Renewable Energy*, 2026, **256**.

27. L. Yang, X. Huang, X. Li, S. Liu, F. Cheng, T. Wen, Z. Kan, Z. Xu and K. Hu, *Fuel*, 2026, **405**.